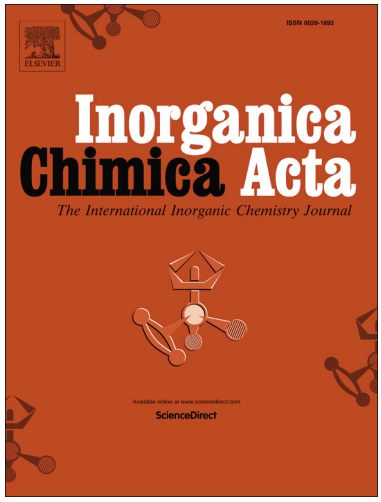


Research paper

# A new anionic metal-organic framework based on tetranuclear zinc clusters: selective absorption of $CO_2$ and luminescent response to lanthanide (III) ions

Ai-Ling Cheng, Juan Zhang, Ling-Ling Ren, En-Qing Gao

PII: S0020-1693(18)30027-6
DOI: https://doi.org/10.1016/j.ica.2018.05.039
Reference: ICA 18290

To appear in: *Inorganica Chimica Acta*

Received Date: 5 January 2018
Revised Date: 1 May 2018
Accepted Date: 28 May 2018

Please cite this article as: A-L. Cheng, J. Zhang, L-L. Ren, E-Q. Gao, A new anionic metal-organic framework based on tetranuclear zinc clusters: selective absorption of $CO_2$ and luminescent response to lanthanide (III) ions, *Inorganica Chimica Acta* (2018), doi: https://doi.org/10.1016/j.ica.2018.05.039

# A new anionic metal-organic framework based on tetranuclear zinc clusters: selective absorption of $CO_2$ and luminescent response to lanthanide (III) ions

Ai-Ling Cheng[a,*], Juan Zhang[a], Ling-Ling Ren[a], En-Qing Gao[b]

[a] *College of Chemistry and Molecular Engineering, East China Normal University, Shanghai 200240, PR China.*

[b] *Shanghai Key Laboratory of Green Chemistry and Chemical Processes, College of Chemistry and Molecular Engineering, East China Normal University, Shanghai 200062, PR China.*

**Corresponding authors.*

*Email address:* alcheng@chem.ecnu.edu.cn (A.-L. Cheng)

Keywords: anionic; metal-organic framework; ultra-microporous; gas adsorption; luminescent

Abstract: A new anionic metal-organic framework, $\{[H_3O]_2[Zn_4(\mu_4\text{-}O)(NSBPDC)_4]\cdot 16(H_2O)]\}_n$ **(1)**, was synthesized under solvothermal conditions using a predesigned multifunctional dicarboxylic acid ($H_2$NSBPDC = 6-nitro-2,2'-sulfone-4,4'-dicarboxylic acid**)**. Complex **1** contains 4-connected tetrahedral $[Zn_4(\mu_4\text{-}O)(CO_2)_8]$ clusters, which are further linked by the bridging ligands, generating a three-fold interpenetrated diamond-like network with ultra-microporous channels. Gas adsorption studies reveal that **1** has good adsorption selectivity for $CO_2$ over $CH_4$ and $N_2$. In addition, **1** can serve as a host to incorporate lanthanide cations via a targeted ion-exchanged process. Notably, the structure of **1** can be dehydrated and rehydrated reversibly.

## 1. Introduction

Metal−organic frameworks (MOFs), as a new class of hybrid organic-inorganic materials, has attracted considerable attention owing to their structural diversity and promising applications in adsorption and separation, ion-exchange, catalysis, sensing and so on [1-8]. Therefore, a plethora of MOFs with intriguing structures have been constructed by rational selection of metal ions (or metal clusters) and organic ligands [9-11]. Significantly, polynuclear metal clusters (di-, tri-, tetranuclear and even higher-nuclear clusters) usually possess high rigidity and well-established geometries, which can be viewed as secondary building units (SBUs) to construct robust high-connected MOFs with predictable topologies [12-14]. Among the various kinds of SBUs, dinuclear copper and tetranuclear zinc clusters have been widely studied for the generation of desirable MOFs. In particular, with the 6-connected octahedral $[Zn_4O(COO)_6]$ as SBUs, a series of **pcu** type MOFs (IRMOFs) have been successfully synthesized by using different linear decarboxylases as the ligands [13]. Additionally, by replacing the linear dicarboxylates with slightly bent ligands [fluorene-2,7-dicarboxylate and *N*,*N*′-bis(4-carboxyphenyl)urea], a rare 3D **kag** type framework (**2**) and an unconventional flexible pcu type framework (**3**) based on $[Zn_4O(COO)_6(sol)_2]$ (sol = DMSO/DMF) clusters have been obtained, respectively [15, 16]. The above results indicate that the slight bending of the dicarboxylate ligands would affect the

connection mode of the $Zn_4O$ cluster and then lead to different topologies. However, MOFs constructed from polynuclear clusters as nodes and slightly bent dicarboxylates as linkers are still limited.

On the other hand, technologies for $CO_2$ capture become increasingly significant in both academic researches and industrial applications [17, 18]. In general, adsorption capacity and selectivity are two main aspects to evaluate an adsorbent material for $CO_2$ capture. Compared with traditional porous adsorbent materials, MOFs have shown prominent advantages for potential applications in $CO_2$ capture, owing to their extra-high porosity and tunable pore environments [19-22]. In recent decades, great efforts have been made to improve the adsorption properties of MOFs for $CO_2$, and several efficient strategies have been developed [23-26]. For one thing, regulation of pore size distribution. Recent studies suggested that MOFs featuring ultra-micropores (< 7 Å) are applicable for separating gases with similar diameters during which the separation process is mainly based on molecular sieving effect [26]. For another, on account of the intrinsic quadruple moment and weak acidity of $CO_2$ molecules, the affinity of adsorbents toward $CO_2$ can be enhanced by the following methods: functionalization of the pore walls with basic or polar functional groups, such as $–NH_2$, $–NO_2$, –CN, and so on; introduction of unsaturated coordinated metal centers (UMCs); incorporation of electrostatic fields by design of charged skeletons. Though some progress has been achieved in this domain, the relevant research is still far from enough. The enhanced host–guest interactions and molecular sieve effect may enhance the adsorption performance cooperatively, which can be realized by construction of MOFs featuring ultra-microporosity, functional group decoration and charged skeleton.

In addition, MOFs decorated with functional groups can be applied not only to selective $CO_2$ separation, but also to some special areas including molecular recognition and catalysis [27]. Recently, we and others have reported series of sulfone-functionalized MOFs assembled from metal motifs and a slightly bent functional dicarboxylate ligand, 2,2'-sulfone-4,4'-dicarboxylic acid ($H_2$SBPDC), some of which showed guest-responsive photoluminescence and gas adsorption properties [28-33]. Along the line, 6-nitro-2,2'-sulfone-4,4'-dicarboxylic acid ($H_2$NSBPDC) was synthesized and first utilized to react with the zinc ion based on the following reasons: I. the nitro group can increase the polarity of the ligand, which might lead to a stronger affinity of the final framework to $CO_2$; II. The active amino group may be introduced by the follow-on reduction of the nitro group via the chemical modifications; III. Due to the facile tendency of zinc ions to assemble clusters, it is possible to construct novel frameworks based on zinc clusters. In this contribution, we report a new 3D porous framework, $\{(H_3O)_2][Zn_4O(NSBPDC)_4]\cdot 16(H_2O)\}_n$ (**1**), which is a three-fold interpenetrated diamond-like anionic network based on 4-connected $[Zn_4O(COO)_8]$ clusters. As we expected, complex **1** not only shows good adsorption selectivity for $CO_2$ over $CH_4$ and $N_2$, but also can serve as a host to incorporate $Ln^{3+}$ ions by cation-exchange. Additionally, the structure of **1** exhibits a reversible dehydration and rehydration process.

## 2. Experimental

2.1 Materials and methods

All reagents were purchased commercially and used without further purification. 6-nitro-2,2'-sulfone-4,4'-dicarboxylic acid ($H_2$NSBPDC) was prepared according to the literature procedure [34], and the synthetic route is depicted in Scheme S1. The detailed description of the general methods and X-ray Crystallography can be seen in the supporting information. The crystal data of **1**: Tetragonal, $I4_1/a$, T = 296(2) K, $a = b$ = 30.2890(14) Å, $c$ = 8.1594(8) Å, $\alpha = \beta = \gamma$ = 90°, $V$ = 7485.6(9) Å$^3$, $Z$ = 16, no. of reflns measured = 47276, no. of independent reflns = 4671, $R_{int}$ = 0.0473, GOF = 1.051, R ($(I) > 2\sigma(I)$) = 0.0417, w$R$ ($F_o^2$) = 0.1225.

2.2 Synthesis of $\{(H_3O)_2[Zn_4O(NSBPDC)_4]\cdot 16(H_2O)\}_n$ (**1**)

A mixture of $H_2$NSBPDC (20 mg, 0.057 mmol) and $Zn(NO_3)_2\cdot 6H_2O$ (40 mg, 0.13 mmol) in $H_2O$ (8 mL) and $CH_3OH$ (3 mL) was stirred for 30 min in air at room temperature. The mixture was then transferred and sealed in a 23 mL Teflon-lined autoclave, and heated at 172 °C for 5 days. After cooling to ambient temperature slowly, pale brown needle crystals were isolated (55% yield based on $H_2$NSBPDC). Anal. Calcd. (%) for $C_{56}H_{58}N_4O_{51}S_4Zn_4$: C 33.7, H 2.94, N 2.81. Found: C 32.9, H 2.90, N 2.62%. ICP analysis for $C_{56}H_{58}N_4O_{51}S_4Zn_4$: Zn 13.2%, found: Zn 13.1%. IR data (KBr, cm$^{-1}$): 1602s, 1538m, 1441w, 1388vs, 1178w, 1317，1193，1143.

2.3 Encapsulation of $Ln^{3+}$ in **1**

The as-synthesized **1** (40 mg) was soaked in $H_2O$-methanol (2 mL/1 mL) solutions of $Ln(NO_3)_3$ (0.3 mol·L$^{-1}$, $Ln^{3+}$ = $Eu^{3+}$, $Tb^{3+}$) at 50℃ for 3 days. The exchanged samples were filtrated and thoroughly washed with water, and then dried in air to give $Ln^{3+}$@**1**.

**3. Results and Discussion**

3.1 Description of the crystal structure

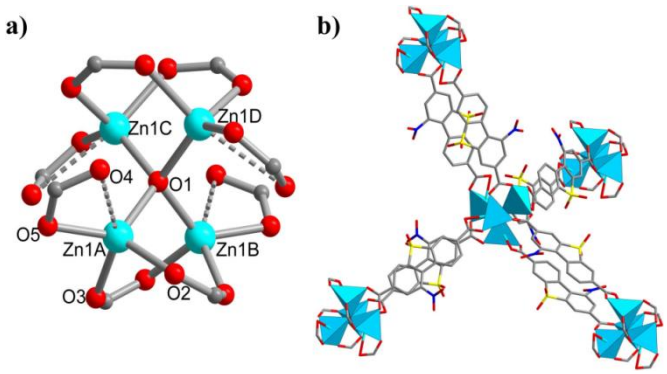


**Fig. 1** Views showing the tetranuclear $[Zn_4O(COO)_8]$ SBU (a) and the pseudo-tetrahedral connectivity of four SBUs in **1** (b) . Hydrogen atoms have been omitted for clarity.

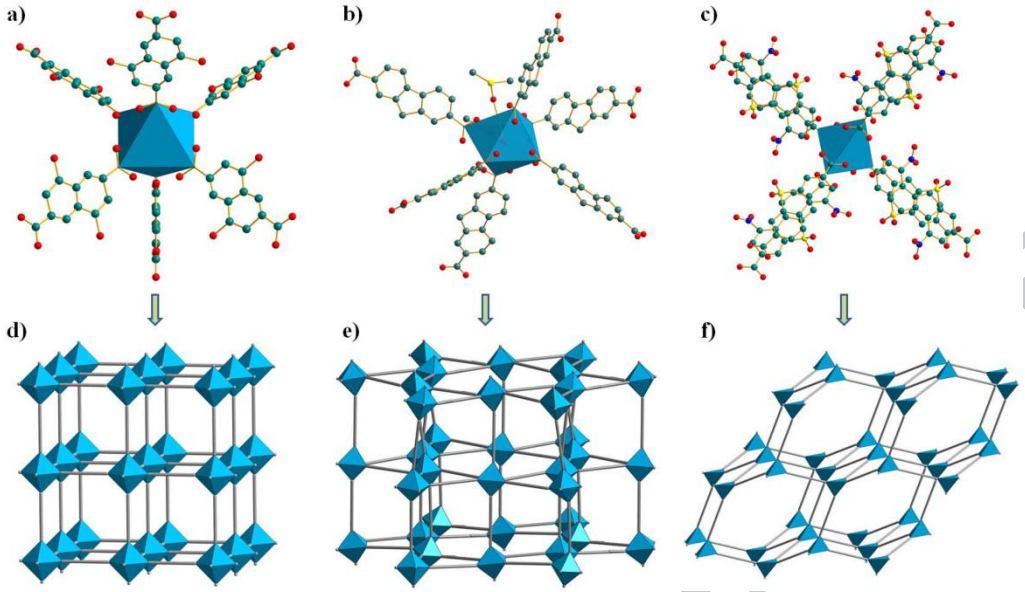


**Fig. 2** Views showing the evolution of the pcu net (d), the kag net (e) and the diamond net (f) constructed by the $Zn_4O$ SBU (a~c) in IRMOFs, **2** and **1**, respectively.

Single-crystal X-ray diffraction analysis indicated that compound **1** crystallizes in the tetragonal space group $I4_1/a$ and features a 3-fold interpenetrated 3D anionic diamond network base on tetranuclear $[Zn_4O(COO)_8]$ clusters. In the cluster, each $Zn^{II}$ ion (Zn1) resides at a crystallographic $\bar{4}$ site, and is surrounded by three carboxylate oxygen atoms from different $NSBPDC^{2-}$ ligands and a central $\mu_4$-O atom, generating a distorted tetrahedral geometry (Fig. 1a). The Zn–O bond lengths are in the range of 1.946–2.009 Å, and the O-Zn-O angles range from 97.14 to 127.40°. In addition, there is one carboxylate oxygen atom (O5) which is coordinated weakly to Zn1 with the Zn–O distance of 2.616 Å. Take into account the weak interaction, the coordination geometry around Zn1 may be considered as a highly distorted square pyramidal geometry. Furthermore, four Zn atoms are connected by one $\mu_4$-O to afford a distorted $[Zn_4O]$ tetrahedron. The Zn···Zn distances are in the range of 2.919–3.321 Å, and the Zn-O-Zn angles range from 96.6° to 116.3°.

It is noteworthy that the clusters in **1** are different from the well-known $[Zn_4O(COO)_6]$ clusters in IRMOFs [13] and $[Zn_4O(COO)_6(DMSO)_2]$ clusters in MOF (**2**) [15]. In each cluster of the IRMOF-n series (Fig. 2a), four Zn atoms form an ideal tetrahedron around $\mu_4$-O. There is one $\mu_2$-carboxylate bridge on each edge of the $Zn_4O$ tetrahedron, generating a 6-connected regular octahedral SBU with the $O_h$ symmetry. Then, the clusters are interlinked by the linear linkers to give a 3D framework with **pcu** topology (Fig. 2d). As for **2**, the $Zn_4O$ cluster is also furnished by six $\mu_2$-carboxylate bridges at the six edges, but the coordination of the additional DMSO molecules to two Zn ions leads to a distorted $Zn_4O$ tetrahedron (Fig. 2b) and a distorted octahedral 6-connected SBU with the pseudo-$D_{2h}$ symmetry. The equatorial inter-link angles of the SBU deviate significantly from 90° to 60° and 120°, which leads to the formation of a framework with the kag topology (Fig. 2e). Differently, in each $Zn_4O$ cluster of **1** (Fig. 1b, 2c), two nonadjacent edges (Zn1A···Zn1B and Zn1C···Zn1D) of the tetrahedron is each bridged by two $\mu_2$-carboxylate groups (Zn···Zn 2.919 Å, Zn-O-Zn 96.6°), but no carboxylate bridge is involved in the remaining

four edges (Zn···Zn 3.321 Å, Zn-O-Zn 116.3°). Besides, each vertex of the tetrahedron is chelated by one carboxylate group. As a result, each $Zn_4O$ cluster is furnished by eight carboxylate groups (four bridging and four chelating). Instead of serving as 8-connected node, the $[Zn_4O(COO)_8]$ SBU is 4-connected, with a pair of the dicarboxylate ligands as double linkers between neighboring SBU (Fig. 1b). Each ligand binds one $Zn_4O$ cluster in a bidentate chelating fashion and another cluster in a bidentate bridging mode. The overall network of **1** shows the well-known diamond (dia) topology (Fig. 2f, 3a). Owing to the large void generated in a single net, three identical nets mutually interpenetrate in a normal way to generate a 3-fold interpenetrating architecture (Fig. 3b) [35]. Notably, despite the interpenetration, the framework still exist 1D channels along the *c*-axis with dimensions of 5.6 Å × 5.6 Å (measured between opposite oxygen atoms of nitro groups with consideration of van der Waals radii) (Fig. 4a). Based on the PLATON [36] calculations, the void value of the channels comprises 23.3% of the crystal volume (1745.5 $Å^3$ out of 7485.6 $Å^3$ unit cell volume), in which the disordered $H_3O^+$ counterions and $H_2O$ molecules are filled. Combined with the charge balance considerations, TG and elemental analyses, the chemical formula of **1** is determined as $\{(H_3O)_2[Zn_4O(NSBPDC)_4]\cdot 16(H_2O)\}_n$.

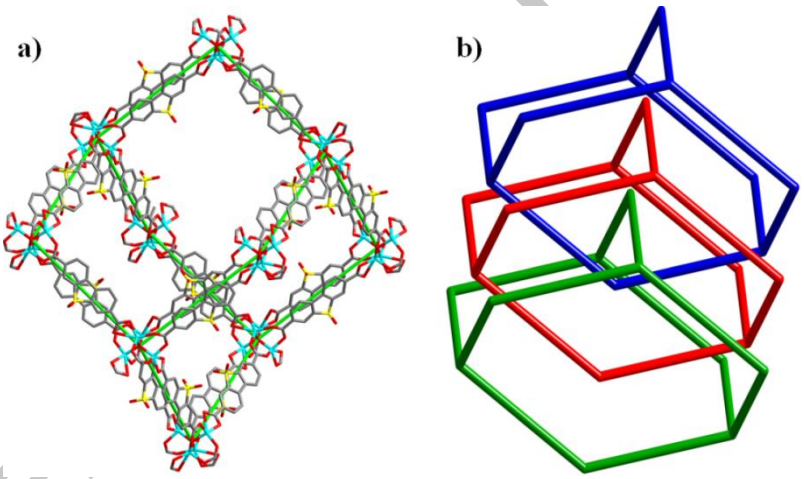


**Fig. 3** Views showing the diamond network (a) and 3-fold interpenetration of the network (b) in **1.** Hydrogen atoms and nitro groups in figure 3a are emitted for clarity.

Additionally, the diamond coordination framework and the 3-fold interpenetration is sustained by extended interplanar π–π interactions (Fig. 4b). In particular, the two ligands that constitute the double linkers between two SBUs are parallel with interplanar and centroid–centroid distances of 3.8 Å and 4.0 Å. Additionally, each ligand from one net stack in parallel to a neighboring ligand from another net, with interplanar and centroid–centroid distances of 3.5 Å and 3.7 Å. Thus it can be seen that the ligands form infinite π–π stacking arrays along the *c* direction. The structure around a channel can be regarded as three double-stranded helical chains extending around the $4_1$ screw axes in an ABCABC fashion along the *c* direction (A, B, C represent the double-stranded helical chains from the three interpenetrated networks). Remarkably, all of the nitro and sulfo-functional groups of the ligands are dangled on the inner walls of these channels, which might provide uniform sites for host-guest interactions.

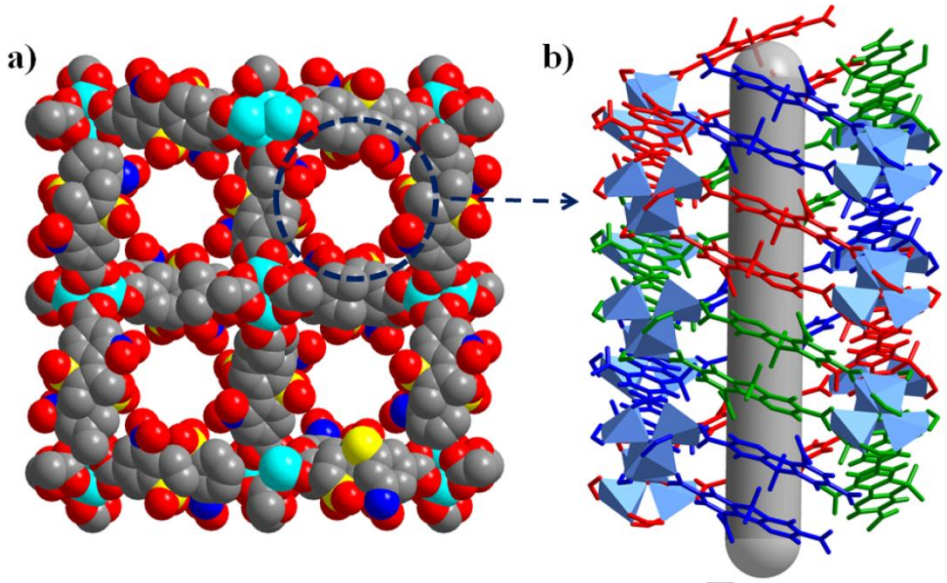


**Fig. 4** Views showing the 1d channels along the *c* axis (a) and the parallel spiral packing of the double linkers around a channel (b) in **1.**

Inspections into the framework of **1** suggest that the functional groups (-$SO_2$, -$NO_2$) might have critical impacts on the packing mode of the structure. The electron drawing effect of the functional groups might enhance the π-π stacking interactions between the benzene rings of the bridging ligands, and the pairwise π-π stacking tends to arrange the linkers in parallel, leading to such a diamond-like three-fold interpenetrated network based on 4-connected tetrahedral [$Zn_4(\mu_4\text{-}O)(CO_2)_8$] clusters.

3.2 Rehydration studies

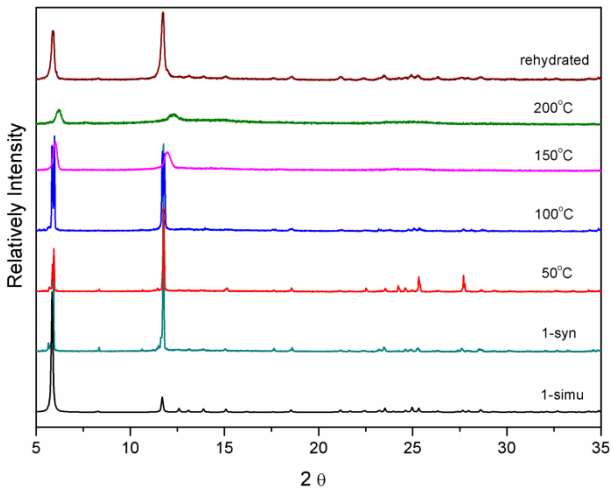


Fig. 5 PXRD patterns for complex 1.

As shown in Fig. 5, the PXRD patterns of as-synthesized samples of **1** match well with the simulated one, indicating the good phase purity of compound **1**. Thermo gravimetric analysis (TGA) of **1** shows a weight loss of 15.4% (calc. 16.2%) from 50°C to 200 °C, corresponding to the loss of eighteen $H_2O$ molecules, and the framework begins to decompose above 350 °C (Fig.

S6). In addition, PXRD experiments under different temperatures were also performed to investigate the thermal behavior of **1** upon removal of guest molecules. The studies show that the framework begins to collapse upon heating at 150 °C (Fig. 5), which means that **1** loses its crystallinity along with the loss of guest molecules. Presumably, along with the release of the $H_2O$ molecules, protons liberated from $H_3O^+$ will combine with carboxylate groups, and the coordination interactions between carboxylates and $Zn^{2+}$ ions will be weakened. This might be one of the reasons for the collapse of the framework. However, the crystallinity of **1** can be regained by exposing the amorphous material to water vapor for several hours at room temperature. The above results indicate that the framework of **1** can be dehydrated and rehydrated reversibly.

3.3 Gas adsorption properties

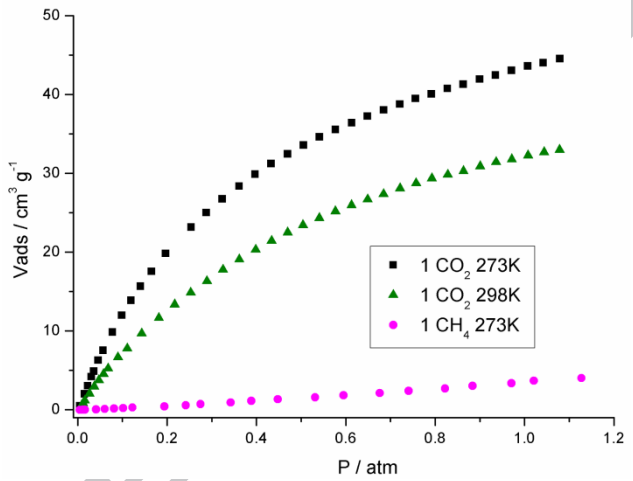


**Fig. 6** Gas adsorption isotherms of $CO_2$ and $CH_4$ for **1** at 273K and 298K.

The presence of the charged skeleton and the polar group decorated pores encourage us to explore the selective adsorption properties of **1** for $CO_2$. To prove our hypothesis, the sorption behavior of $CO_2$ and $CH_4$ were investigated at 273 K (Fig. 6). Prior to gas sorption experiments, compound **1** was activated at 100 °C under vacuum for 6h. The largest uptake values for $CO_2$ and $CH_4$ are 44.5 $cm^3 g^{-1}$ and 4.1 $cm^3 g^{-1}$ at 1 atm, and the uptake capacity of **1** for $CO_2$ is 10.9 times higher than that for $CH_4$. Moreover, $N_2$ adsorption experiment shows that **1** does not adsorb $N_2$ molecules (Fig S7). The results suggest that **1** may be suitable for the separation of $CO_2$ over $CH_4$ and $N_2$.

To further estimate the affinity of the framework toward $CO_2$, the isosteric enthalpies of $CO_2$ adsorption ($Q_{st}$) were calculated by the Clausisus–Clapeyron equation. At zero coverage, the $Q_{st}$ value for $CO_2$ was 39.1 $kJ \cdot mol^{-1}$ (Fig. S8), which indicates that the interactions between the framework of **1** and $CO_2$ molecules are relatively strong. Noticeably, the $Q_{st}$ value of **1** exceeds that of many reported MOFs featuring UMCs or charged skeletons, such as HKUST-1 (29.2 $kJ \cdot mol^{-1}$) [37], CPF-13 (28.2 $kJ \cdot mol^{-1}$) [38] and $[(CH_3)_2NH_2]_3[(Cu_4Cl)_3(BTC)_8] \cdot 9DMA$ (25.38 $kJ \cdot mol^{-1}$ ) [39]. The high $Q_{st}$ value and good adsorption selectivity of $CO_2/CH_4$ of **1** could be attributed to the following two aspects: Firstly, the narrow pore size distribution of **1** (5.6 Å) suggests that molecular sieve effect might play a key role for the high adsorption affinity.

Secondly, the interactions between the framework and adsorbed $CO_2$ molecules (quadrupole moment $-1.4\times10^{-39}$ $Cm^2$) can be further enhanced through charge-induced forces owing to the presence of the decorated polar groups and charged skeleton. Moreover, there might be a synergistic effect between the above two factors. Additionally, the low adsorption affinity of **1** toward $CH_4$ (perhaps caused by the low polarity of $CH_4$) can be confirmed by the near-linear adsorption isotherm of $CH_4$ [24].

3.4 Encapsulation of $Ln^{3+}$ ions

As described above, the anionic framework of **1** contains 1D channels dispersed with $H_3O^+$ cations, which makes it suitable for fabrication of Ln-doped luminescent materials via encapsulation of lanthanide cations. To load the $Ln^{3+}$ cations into the pores of **1**, the solid sample of **1** was immersed in methanol/$H_2O$ (1/2 v/v) solution containing $Ln(NO_3)_3$ (0.3 mol·$L^{-1}$, 50℃) for ion exchange. As confirmed by ICP date, the doped amount of $Ln^{3+}$ ions is about 8.07% for $Tb^{3+}$ and 5.72% for $Eu^{3+}$ (mol% compared with $Zn^{2+}$ ions), indicating that only a few parts of $H_3O^+$ cations have been exchanged by $Ln^{3+}$ ions. The PXRD patterns of the $Ln^{3+}$@**1** samples are almost identical with that of the as-synthesized **1** (Fig. S9), which confirmed that the crystalline integrity of the structure was maintained upon the lanthanide adsorption. Besides, the PXRD patterns for $Ln^{3+}$@**1** shows two additional sets of peaks at slightly different values, suggesting that a subtle structural change happens along with the encapsulation of $Ln^{3+}$. However, the framework of 1 will collapse irreversibly when continue to raise the ion-exchange temperature (Fig. S10).

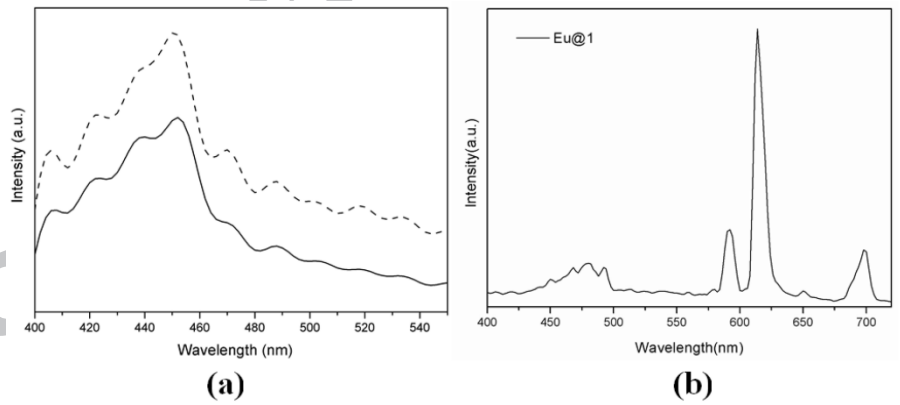


**Fig. 7** (a) Solid-state emission spectra of $H_2$NSBPDC and **1** ($\lambda_{ex}$ = 290 nm); (b) Emission spectra of Eu@**1** ($\lambda_{ex}$ = 327 nm).

In addition, the solid emission properties of $H_2$NSBPDC, **1** and Ln@**1** were investigated at room temperature (Fig 7). As shown in Fig. 7a, compound **1** exhibits strong blue emission with a maximum at 450 nm upon excitation at 290 nm, which is in accordance with that of the free $H_2$NSBPDC ligand ($\lambda_{em}$ = 452nm, $\lambda_{ex}$ = 290nm). Thus, the luminescence of **1** can be attributed to the intra-ligand ($\pi\rightarrow\pi$ *) charge transitions. In the case of $Eu^{3+}$@**1**, the emission bands at 578 nm, 591 nm, 614 nm, 649 nm and 694 nm are consistent with the typical $Eu^{3+}$ ion emissions ($\lambda_{ex}$ = 327 nm), which are ascribed to $^5D_0\rightarrow{}^7F_J$ (J = 0~4) transitions. The strongest emission peak at 614 nm

can be assigned to the $^5D_0 \rightarrow {}^7F_2$ transition. Simultaneously, the characteristic emission of **1** at 450nm still retained, indicating that only part of the energy is transferred from **1** to the $Eu^{3+}$ centers. As for $Tb^{3+}$@**1**, the characteristic emissions of $Tb^{3+}$ were not observed probably due to the mismatch of the energy levels of **1** and $Tb^{3+}$.

## 4. Conclusions

In conclusion, an new anionic MOF (**1**) was constructed from 4-connected tetrahedral $[Zn_4O(COO)_8]$ clusters and a predesigned functional ligand ($H_2$NSBPDC). Complex **1** is a 3-fold interpenetrated diamond-like network featuring 1D ultra-microporous channels. Gas adsorption measurements showed that the adsorption heat for $CO_2$ is relatively very high, and **1** could be suitable for selective separation of $CO_2$ over $CH_4$ and $N_2$. The results reveal that the molecular sieve effect and enhanced host–guest interactions can cooperatively improve the $CO_2$ capture performance. In addition, **1** can adsorb $La^{3+}$ ions via a targeted ion-exchanged process to form red luminescent materials. These results will facilitate the exploration of novel multi-functional materials for selective $CO_2$ adsorption and light emission.

## Notes

The authors declare no competing financial interest.

## Acknowledgements

This work is financially supported by the National Natural Science Foundation of China (Grant no. 21201064).

## Appendix A. Supplementary data

Supplementary data associated with this article can be found, in the online version,

## Notes and references

1. P. Falcaro, R. Ricco, C. M. Doherty, K. Liang, A. J. Hill, M. J. Styles, Chem. Soc. Rev. 43 (2014) 5513-5560.
2. Y. -B. Huang, J. Liang, X. -S. Wang, R. Cao, Chem. Soc. Rev. 46 (2017) 126-157.
3. W. Li, Y. Zhang, Q. Li, G. Zhang, Chem. Eng. Sci. 135 (2015) 232-257.
4. J. Liu, L. Chen, H. Cui, J. Zhang, L. Zhang, C. -Y. Su, Chem. Soc. Rev. 43 (2014) 6011-6061.
5. W. P. Lustig, S. Mukherjee, N. D. Rudd, A. V. Desai, J. Li, S. K. Ghosh, Chem. Soc. Rev. 46 (2017) 3242-3285.
6. Z. Zhang, Z.-Z. Yao, S. Xiang, B. Chen, Energ. Environ. Sci. 7 (2014) 2868-2899.

7. D. Zhao, Y. Cui, Y. Yang, G. Qian, CrystEngComm 18 (2016) 3746-3759.
8. P. Silva, S. M. Vilela, J. P. Tome, F. A. Almeida Paz, Chem. Soc. Rev. 44 (2015) 6774-6803.
9. C. Sanchez, C. Boissiere, S. Cassaignon, C. Chaneac, O. Durupthy, M. Faustini, D. Grosso, C. Laberty-Robert, L. Nicole, D. Portehault, F. Ribot, L. Rozes and C. Sassoye, Chem. Mater. 26 (2013) 221-238.
10. Y. Sun, H. -C. Zhou, Sci. Technol. Adv. Mat. 16 (2015) 1-11.
11. W.-X. Zhang, P.-Q. Liao, R.-B. Lin, Y.-S. Wei, M.-H. Zeng, X.-M. Chen, Coord. Chem. Rev. 293 (2015) 263-278.
12. M. Zhang, G. Feng, Z. Song, Y. -P. Zhou, H. -Y. Chao, D. Yuan, T. -T. Tan, Z. Guo, Z. Hu, B. -Z. Tang, B. Liu, D. Zhao, J. Am. Chem. Soc. 136 (2014) 7241-7244.
13. M. Eddaoudi, J. Kim, N. Rosi, D. Vodak, J. Wachter, M. O'Keeffe, O. M. Yaghi, Science 295 (2002) 469-472.
14. D. Bradshaw, J. B. Claridge, E. J. Cussen, T. J. Prior, M. J. Rosseinsky, Acc. Chem. Res. 38 (2005) 273-282.
15. Q. Yue, Q. Sun, A.-L. Cheng, E.-Q. Gao, Cryst. Growth Des. 10 (2010) 44-47.
16. R. J. Marshall, J. McGuire, C. Wilson, R. S. Forgan, Supramol. Chem. 30 (2018) 124-133.
17. E. S. Sanz-Perez, C. R. Murdock, S. A. Didas, C. W. Jones, Chem. Rev. 116 (2016) 11840-11876.
18. A. L. Yaumi, M. Z. A. Bakar, B. H. Hameed, Energy 124 (2017) 461-480.
19. Y. S. Bae, R. Q. Snurr, Angew. Chem. Int. Ed. 50 (2011) 11586-11596.
20. E. González-Zamora, I. A. Ibarra, Mater. Chem. Front. 1 (2017) 1471-1484.
21. K. Sumida, D. L. Rogow, J. A. Mason, T. M. McDonald, E. D. Bloch, Z. R. Herm, T. H. Bae, J. R. Long, Chem. Rev. 112 (2012) 724-781.
22. J. Yu, L. -H. Xie, J. -R. Li, Y. Ma, J. M. Seminario, P. B. Balbuena, Chem. Rev. 117 (2017) 9674-9754.
23. L. Kong, R. Zou, W. Bi, R. Zhong, W. Mu, J. Liu, R. P. S. Han, R. Zou, J. Mater. Chem. A 2 (2014) 17771-17778.
24. R. Zhong, Z. Xu, W. Bi, S. Han, X. Yu, R. Zou, Inorg. Chim. Acta 443 (2016) 299-303.
25. L. Du, Z. Lu, K. Zheng, J. Wang, X. Zheng, Y. Pan, X. You, J. Bai, J. Am. Chem. Soc. 135 (2013) 562-565.
26. P. Nugent, Y. Belmabkhout, S. D. Burd, A. J. Cairns, R. Luebke, K. Forrest, T. Pham, S. Ma, B. Space, L. Wojtas, M. Eddaoudi, M. J. Zaworotko, Nature 495 (2013) 80-84.
27. B. Li, M. Chrzanowski, Y. Zhang, S. Ma, Coord. Chem. Rev. 307 (2016) 106-129.
28. E. Neofotistou, C. D. Malliakas, P. N. Trikalitis, Chemistry 15 (2009) 4523-4527.
29. E. Neofotistou, C. D. Malliakas, P. N. Trikalitis, CrystEngComm 12 (2010) 1034-1037.
30. I. Spanopoulos, P. Xydias, C. D. Malliakas, P. N. Trikalitis, Inorg. Chem. 52 (2013) 855-862.
31. S. Xiong, S. Wang, X. Tang, Z. Wang, CrystEngComm 13 (2011) 1646-1653.
32. P. Xydias, I. Spanopoulos, E. Klontzas, G. E. Froudakis and P. N. Trikalitis, Inorg. Chem. 53 (2014) 679-681.
33. L. Yan, Q. Yue, Q.-X. Jia, G. Lemercier, E.-Q. Gao, Cryst. Growth Des. 9 (2009) 2984-2987.

34. V. K. Olkhovik, D. A. Vasilevskii, A. A. Pap, G. V. Kalechyts, Y. V. Matveienko, A. G. Baran, N. A. Halinouski, V. G. Petushok, Arkivoc (2008) 69-93.

35. S. R. Batten, CrystEngComm 18 (2001) 1-7.

36. A. L. Spek, J. Appl. Cryst. 36 (2003) 7-13.

37. S. Bordiga, L. Regli, F. Bonino, E. Groppo, C. Lamberti, B. Xiao, P. S. Wheatley, R. E. Morris, A. Zecchina, Phys. Chem. Chem. Phys. 9 (2007) 2676-2685.

38. Q.-G. Zhai, Q. Lin, T. Wu, L. Wang, S.-T. Zheng, X. Bu, P. Feng, Chem. Mater. 24 (2012) 2624-2626.

39. Y.-X. Tan, Y.-P. He, J. Zhang, Chem. Commun. 47 (2011) 10647-10649.

**Graphical Abstracts**

**A new anionic metal-organic framework based on the $[Zn_4(\mu_4\text{-}O)(CO_2)_8]$ clusters: selective absorption of $CO_2$ and luminescent response to lanthanide (III) ions**

Ai-Ling Cheng[a,*], Juan Zhang[a], Ling-Ling Ren[a], En-Qing Gao[b]

An anionic MOF containing ultra-microporous channels decorated with polar groups is synthesized and its selective adsorption properties are explored.

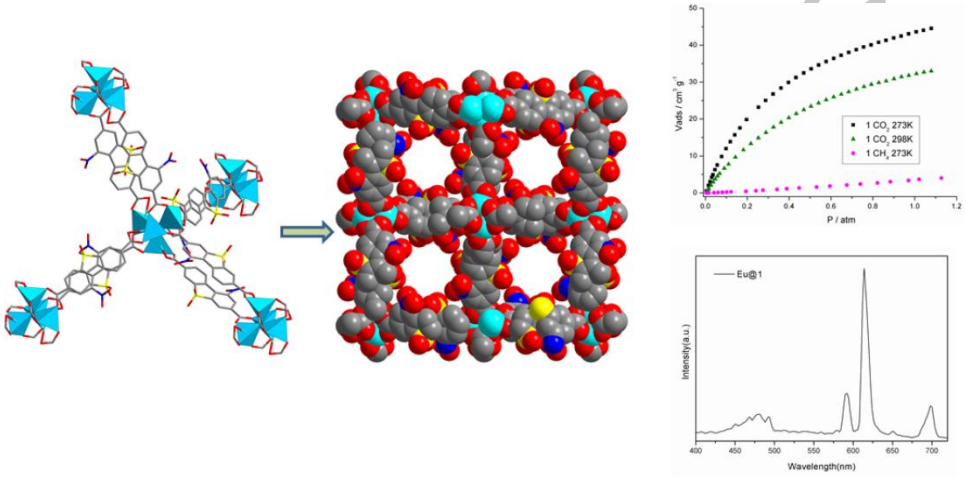

Research Highlights

- A new anionic MOF (**1**) based on $[Zn_4(\mu_4\text{-}O)(CO_2)_8]$ clusters was synthesized.
- The structure of **1** can be dehydrated and rehydrated reversibly.
- **1** has good adsorption selectivity for $CO_2$ over $CH_4$ and $N_2$.